

# **A Novel Ultrasonic Method for Measuring the Position and Velocity of Moving Objects in 3D Space**

Natee Thong-un, Wongsakorn Wongsaroj<sup>\*</sup>

Department of Instrumentation and Electronics Engineering, King Mongkut's University of Technology North Bangkok, Bangkok, Thailand

Received 05 January 2022; received in revised form 27 January 2022; accepted 05 February 2022

DOI: <https://doi.org/10.46604/aiti.2022.9396>

## **Abstract**

This study proposes a method for concurrently determining the position and velocity of a moving object in three-dimensional (3D) space using echolocation. A spherical object, i.e., a flying ball, is used to demonstrate the ability of the proposed method. The position of the object is calculated using a time-of-flight (TOF) technique based on a cross-correlation function, which requires less computational time when using one-bit signal technology. The velocity of the object is subsequently computed from the length of chirp signals and the velocity vector measurements between the position of the object and the position of acoustical receivers. The coordinate of the object location is identified by the distance from the sound source to the object, the elevation angle, and the azimuth angle. The validity and repeatability of the experimental results are evaluated by statistical methods, showing  $\pm 1\%$  of accuracy. It is concluded that the proposed method can identify the position and velocity of a rigid body in 3D space.

**Keywords:** chirp signal, echolocation, one-bit signal, position, velocity

## **1. Introduction**

Bats and dolphins have a remarkable ability to generate an image of the world from acoustic data or called ultrasound, while almost all other animals produce the image from visual information. They can transmit sound pulse trains and identify targets by using echolocation [1]. In engineering measurement, there are many applications of the ultrasonic technique applied such as fluid engineering [2], non-destructive testing [3], and so on. To determine the distance, time-of-flight (TOF) methods are proposed to provide the time interval between the emitted sound and received echo. TOF methods can be used in a variety of applications [4-7]. There are many studies on acoustic systems for position measurement [8-13]. The target position is identified by the TOF computation between the transmitter and the receiver of sound. However, this determination of position does not consider the effects of velocity.

Presently, the most advanced devices for robots use a laser rangefinder and a vision finder. However, these devices still have disadvantages when compared with ultrasonic airborne systems [14]. For instance, the vision system's main disadvantage is the time-consuming computational methods and the high expense of the system [15]. The localization techniques using ultrasonic methods are inexpensive alternatives as suitable ultrasonic transducers can be produced for as little as USD 10 [9]. Moreover, ultrasonic ranging systems can be applied in electromagnetically shielded environments where GPSs cannot be used.

---

<sup>\*</sup> Corresponding author. E-mail address: [wongsakorn.w@eng.kmutnb.ac.th](mailto:wongsakorn.w@eng.kmutnb.ac.th)

Tel.: +66-2-5552000; Fax: +668-4-2356417

Pulse compression signals for ultrasonic methods are an ingenious solution for dealing with the practical problem in ultrasonic TOF measurement because they provide a high level of accuracy [16-17]. In general, a linear-frequency-modulated (LFM) signal can be utilized for TOF computation by using the maximum peak time in the cross-correlation function of the received signal as the reference signal. However, if the LFM signal is heavily modulated by the Doppler effect, it is unsuitable for measuring moving objects. The problem is that cross-correlation cannot completely be achieved between the transmitted signal and the received signal. To overcome this problem, a linear-period-modulated (LPM) signal, which is a pulse compression signal, has been presented [18-19]. Although these methods can satisfy the Doppler effect, they require a lengthy period of computational time because of the use of the envelop-signal calculation.

Accordingly, a low-computation-cost method for ultrasonic distance measurement has been proposed by applying two cycles of pulse compression to LPM signals and compensating for the Doppler-shifted [20-21]. Signal processing-based one-bit stream is the powerful technique of digital decoder for super audio CD (SACD) with direct stream digital (DSD) technology. This processing allows an SACD to achieve its unprecedented audio quality, thus allowing it to reproduce audio better than several digital or analog technologies [22]. In addition, the cross-correlation process of pulse compression signals for TOF computation relies on one-bit signal processing technology [23]. This process is proposed for the accuracy and the resolution of ultrasonic distance measurement as well as hugely reducing the number of multiplications and accumulations of the one-bit signal. Two-dimensional (2D) and three-dimensional (3D) airborne ultrasonic systems using one-bit signal processing have been developed [24, 9], respectively. Unfortunately, the 3D airborne ultrasonic system for one-bit signal processing has a limitation in that it supports only mobile robots with a 90° scanning area and does not include the velocity measurements [25-26].

In a recent development, for instance, Lazarov et al. [27] proposed the design and implementation of the ultrasonic positioning system based on new multifunctional hardware components to visualize the 3D distance of moving objects. However, the measurement technique cannot obtain the object's velocity. To address these critical issues, a direction-of-arrival (DOA) technique is interesting because it essentially concerns the direction of the signal source in 3D positioning, either in the form of an electromagnetic or acoustic wave, when impinging on the sensor array [28]. Also, the object velocity can be estimated by utilizing the technique. Accordingly, the determination of the direction of the echo from an object position using a DOA technique is not complicated, and it can cover a range of  $\pm 180^\circ$  in both the elevation and azimuth angles.

This study proposes a 3D ultrasonic airborne system for concurrently measuring a moving object's position and velocity. The proposed system can compute the position with the accuracy of a DOA technique. The velocity measurement relies on the projection of 3D vector measurements. This system operates using a one-bit signal processing technique with a low computation cost [29] of a field-programmable gate array (FPGA). The repeatability of measurements is measured by the average and the standard deviation from 50 experiments. In the study, the principle of cross-correlation and Doppler compensation via one-bit signal processing is explained in section 2. The model of 3D position and velocity measurements is represented in section 3. Then, in section 4, the measurement results of the proposed system are illustrated and evaluated. Lastly, the conclusion is summarized in section 5.

## 2. Cross-Correlation and Doppler Compensation via One-Bit Signal Processing

### 2.1. Cross-correlation using one-bit signal processing

In the proposed system, the cross-correlation function, which uses one-bit signal processing, consists of the recursive cross-correlation with one-bit signals and the smoothing operation with a finite impulse response (FIR) low-pass filter, as illustrated in Fig. 1. A pair of LPM signals is driven by the sound source. The echo sensed in each microphone is changed into a one-bit stream  $x(m)$  with a delta-sigma modulation. A reference LPM signal is converted into a reference LPM one-bit signal  $s(k)$  by a digital comparator. The cross-correlation function  $c(m)$  is defined as [29]:

$$c(m) = \sum_{k=1}^{M-1} s(M-k) \cdot x(m-k) \quad (1)$$

The cross-correlation operation of Eq. (1) requires a huge number,  $M$ , of multiplication and summation of one-bit signals. Then, the difference in the cross-correlation operation,  $c(m) - c(m-1)$ , is described as [29]:

$$c(m) - c(m-1) = s(M) \cdot x(m) - s(1) \cdot x(m-M) + \sum_{k=1}^{M-1} [s(M-k) - s(M-k+1)] \cdot x(m-k) \quad (2)$$

The  $s(1)$  and  $s(M)$  have values 1 and -1, respectively, owing to  $s(k)$  being the LPM signal transformed to be a one-bit signal. In addition,  $s(k)$  has hundreds of zero cross points  $Z_k$ . There is the same difference in values, either 1 or -1, between any two consecutive zero-cross points  $Z_k$  and  $Z_{k+1}$  in  $s(k)$ . Hence, the values of  $s(M-k) - s(M-k+1)$  can be expressed as [29]:

$$\begin{aligned} 2, \dots, M-k = Z_{2l-1} \\ s(M-k) - s(M-k+1) = -2, \dots, M-k = Z_{2l} \\ 0, \dots, M-k \neq Z_k \end{aligned} \quad (3)$$

where  $l$  is a natural number. The computation of the recursive cross-correlation operation, which is performed by summing the difference in the cross-correlation operation, is expressed as [29]:

$$c(m) = c(m-1) - x(m-M) + 2 \cdot x(m-M+Z_1) - 2 \cdot x(m-M+Z_2) + 2 \cdot x(m-M+Z_3) - \dots - x(m) \quad (4)$$

The computation cost of the recursive cross-correlation operation arises from the integration and summation of the one-bit samples. The number of summation  $Z_{k+2}$  depends on the number of zero-cross points in the LPM signal. Therefore, the computational costs are constant and independent from the altering of sampling frequency. Thus, the recursive cross-correlation operation of one-bit signals can reduce the computational costs of cross-correlation. Moreover, to improve the signal-to-noise ratio (SNR) of  $c(m)$ , the moving average filter performed in the smoothing operation is required to minimize the high-frequency noise in  $c(m)$ . Finally, the TOF can be expressed in terms of the peaks of the cross-correlation.

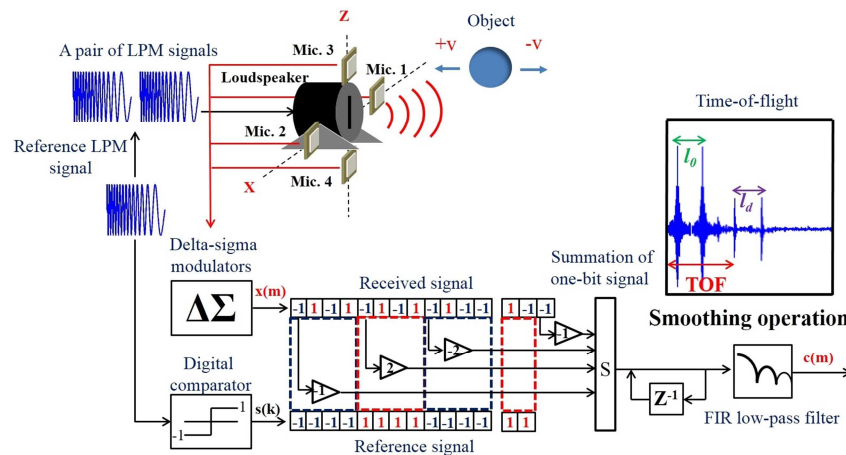


Fig. 1 Proposed three-dimensional position and velocity measurement by one-bit signal processing [29]

## 2.2. Doppler-shift compensation of time-of-flight (TOF)

The TOF of a pair of LPM signals is usually estimated from the time point of the maximum peak in  $c(m)$ . However, considering the case of a moving object, the Doppler effect on the waveform of the modulated cross-correlation function is caused by the phase shift of the received LPM signal, as illustrated in Fig. 2. The maximum peak value in the modulated cross-correlation function does not show the TOF of the received LPM signal. Therefore, the peak time in the envelope of the cross-correlation function  $t_c$  is obtained to estimate the TOF of the received LPM signal.

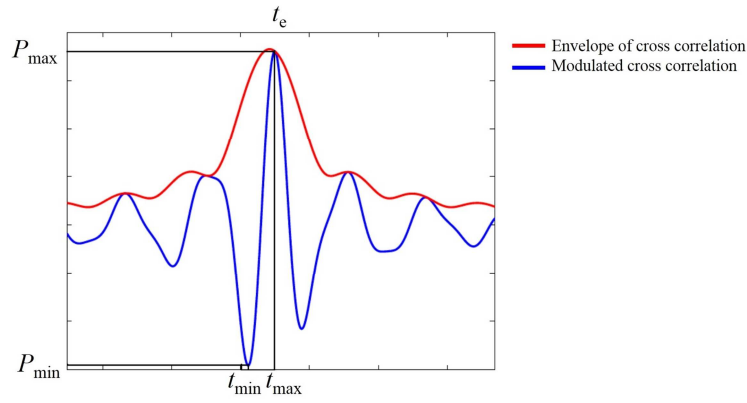


Fig. 2 Modulated cross-correlation envelope of the LPM signal

To identify the TOF due to the cross-correlation, the peak time in the envelope of the cross-correlation function can still be compensated by the maximum peak  $P_{\max}$  and the minimum peak  $P_{\min}$ , the time at the maximum  $t_{\max}$  and minimum  $t_{\min}$ , and the Doppler velocity measurements. The Doppler velocity measurements are required to adjust the length of the modulated LPM signal to account for Doppler effects. The cross-correlation function between the pair of Doppler-shift LPM signals and the single reference LPM signal in Fig. 1 has two peaks. Thus, the interval containing the first maximum peak and the one containing the second maximum peak in the modulated cross-correlation function displays the Doppler-shift length of the single LPM signal. The Doppler-shift length of the reference LPM signal is expressed as [20]:

$$l_d = \frac{v - v_d}{v + v_d} \cdot l_0 \quad (5)$$

where  $l_d$  represents the Doppler-shift length of the received LPM signal,  $l_0$  is the reference LPM signal length,  $v_d$  stands for the Doppler velocity, and  $v$  is the propagation velocity of a sound wave in the air. The original LPM signal  $f(t)$  is defined as [20]:

$$f(t) = \sin \left[ 2\pi \frac{l_0}{p_b} \cdot \ln \left( t + \frac{p_s \cdot l_0}{p_b} \right) - 2\pi \frac{l_0}{p_b} \cdot \ln \left( \frac{p_s \cdot l_0}{p_b} \right) \right] \quad (6)$$

where  $p_b$  is the period of the LPM signal and  $p_s$  is the starting time of the sweeping period. In the work of Hirata et al. [20], the compensated peak time can be estimated from the maximum and minimum peak times and the Doppler velocity coefficient  $\xi$ . For the Doppler velocity in Eq. (7), the compensated peak time is expressed as Eq. (8) [20]:

$$v(e^{\frac{p_b \cdot l}{l_0}} - 1) < v_d < v(e^{\frac{p_b \cdot l+1}{l_0}} - 1) \quad (7)$$

$$\xi = \left| -\frac{2l_0}{p_b} \cdot \ln \left( \frac{v - v_d}{v + v_d} \right) - (2l + 1) \right| \quad (8)$$

$$t_e = \xi \cdot t_{\max} + (1 - \xi) \cdot t_{\min} \quad (9)$$

where  $t_e$  is the compensated peak time and  $l$  is an integer. The TOF of the received LPM signal is estimated as [20]:

$$\text{TOF} = t_e - \frac{v_d}{v + v_d} \cdot \frac{p_s \cdot l_0}{p_b} \quad (10)$$

### 2.3. Direction-of-arrival (DOA)

DOA has been an active method of finding direction for a long time. Typically, the DOA techniques have been found in the application of radar, sonar, and surveillance. They are available for air traffic control and target searching involving the

air-plane industry for converting the location of the transmitter and signal interception. More recently, DOA has played a vital role in mobile radio communications in identifying the multipath of radio channels. DOA is the method based on beamforming in determining the origin of the signal moving to receivers. There are various DOA estimation algorithms such as the algorithms of multiple signal classification (MUSIC) and estimation of signal parameters via rotation invariance technique (ESPRIT). Fig. 3 pictures a pattern of an array with  $M$  elements placed in space. The plane wavefront has a frequency and arrives at an angle  $\theta$  and  $\Phi$  with respect to the  $Z$ -axis and  $X$ -axis, respectively. DOA provides a peak of spectra to match the angle direction come from an original of plane wavefront [28]. This study uses DOA to locate an obstacle.

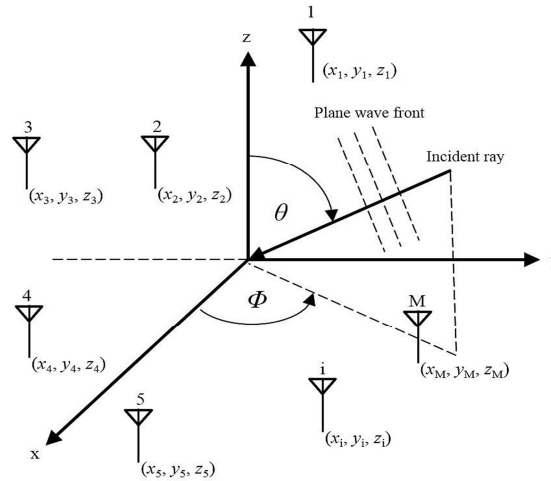


Fig. 3 Basic concept of DOA

### 3. Proposed Model for Three-Dimensional Position and Velocity Measurements

#### 3.1. Three-dimensional position measurements

In Fig. 4(a), the proposed system can detect the object using ranging measurements in an area from  $-X$  to  $+X$  and from  $-Z$  to  $+Z$ . The object is presented in the face of the loudspeaker in  $+Y$  direction. Four acoustical sensors or microphones are located on both the  $X$  and the  $Z$  axes, and their own positions are  $(+m, 0, 0)$ ,  $(-m, 0, 0)$ ,  $(0, 0, +n)$ , and  $(0, 0, -n)$ . The object is supposed to have an unknown position as represented by the point  $(x, y, z)$ .

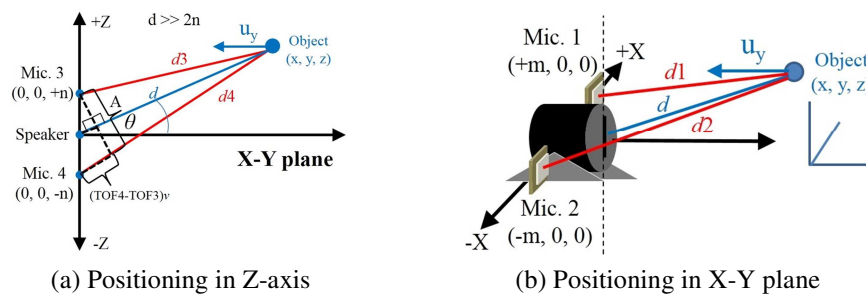


Fig. 4 Three-dimensional positioning method

Firstly, Fig. 4(a) illustrates the object position which is represented in terms of the  $X$ - $Y$  plane and  $Z$ -axis, where  $d$  is the distance from the loudspeaker to the object,  $\theta$  is the elevation angle on the  $X$ - $Y$  plane, and  $2n$  represents the distance between microphones 3 and 4. The object is decided to be whether in  $+Z$  or  $-Z$  direction by evaluating  $TOF_3$  and  $TOF_4$ , which are the TOF as determined by microphones 3 and 4, respectively. If  $TOF_4$  is more than  $TOF_3$ , the object is in the  $+Z$  direction; otherwise, the object is in the  $-Z$  direction. It is supposed that  $d$  is much longer than  $2n$  (i.e.,  $d \gg 2n$ ), which can be deduced from the first triangle secant [30] into the curve in Fig. 4(a). The triangle secant consists of two known sides: the length  $2n$  and the length equal to the difference of the TOF between the microphones 3 and 4 multiplied by the speed of the sound propagation  $v$ . With the definition of DOA, the elevation angle ( $\theta$ ) can be calculated as [31]:

$$\theta = \sin^{-1} \frac{(\text{TOF}_4 - \text{TOF}_3)v}{2n} \quad (11)$$

Secondly,  $d$  is computed by looking back to Fig. 3(a) again. An obtuse triangle with vertex points is created at Mic.4, the speaker, and the target object. Thus,  $d_4$  can be computed as:

$$d_4^2 = d^2 + n^2 - 2nd \cos(90^\circ + \theta) \quad (12)$$

When  $d_4 = v \cdot \text{TOF}_4 - d$ , it is substituted back into Eq. (12).  $d$  can be obtained.

$$d = \frac{(v\text{TOF}_4)^2 - n^2}{2v\text{TOF}_4 - 2n \cos(90^\circ + \theta)} \quad (13)$$

Conversely, if  $\text{TOF}_4$  is less than  $\text{TOF}_3$ , the object occurs in the  $-Z$  direction.  $\theta$  is computed in Eq. (11), but  $d$  is different from that expressed in Eqs. (12) and (13). It can instead be expressed as:

$$d_3^2 = d^2 + n^2 - 2nd \cos(90^\circ + \theta) \quad (14)$$

$$d = \frac{(v\text{TOF}_3)^2 - n^2}{2v\text{TOF}_3 - 2n \cos(90^\circ + \theta)} \quad (15)$$

Now, the parameters  $z$  from  $d$  and  $\theta$  are determined, that is,  $z = d \sin \theta$ . Next, the unknown parameters  $x$  and  $y$  in Fig. 4(b) are considered. The total distance is between the sound source and the object, then to microphone 1, equals  $d + d_1 = v \cdot \text{TOF}_1$ . The parameters  $x$ ,  $y$ , and  $z$  can be related as:

$$y^2 = -x^2 - z^2 - 2mx(v\text{TOF}_1)^2 - 2vd\text{TOF}_1 + d^2 \quad (16)$$

Consider microphone 2, where  $d + d_2 = v \cdot \text{TOF}_2$ , Eq. (17) is obtained similarly to Eq. (16):

$$y^2 = -x^2 - z^2 - 2mx(v\text{TOF}_2)^2 - 2vd\text{TOF}_2 + d^2 \quad (17)$$

Using Eqs. (16) and (17), the  $x$  and  $y$  parameters can be solved. Lastly, a transform from the Cartesian coordinate system to the spherical coordinate system is utilized to obtain the angle of azimuth ( $\phi$ ).

$$\phi = \cos^{-1} \frac{2vd(\text{TOF}_1 - \text{TOF}_2) + v^2(\text{TOF}_2^2 + \text{TOF}_1^2)}{4dm \sin \alpha} \quad (18)$$

### 3.2. Three-dimensional velocity vector measurements

The velocity of the moving object can be measured from the signal length of the echo, which is reflected from the target. The signal length difference is proportional to the velocity of the object. The length of the received LPM signal is linearly decreased or increased due to the Doppler effect. The Doppler velocity at each microphone, which is a relative velocity measurement, can be expressed in Eq. (5). It is assumed that the microphone vectors are the directions in which the microphones measure the relative velocity from the moving object, as illustrated in Fig. 3. These vectors can be computed with the coordinates of the instantaneous object position and the microphone position. If the unknown velocity vector of the moving object  $u = [u_x, u_y, u_z]^T$  is projected onto the microphone vectors, the result of the projection is the relative velocity measured by the microphones. Thus, the velocity of the moving object can be estimated using the measurements from the relative velocity of each microphone, the instantaneous object position of the moving object, and the microphone positions. The relative-Doppler velocity measurements  $V_d = [v_{d1}, v_{d2}, v_{d3}, v_{d4}]^T$  of microphones 1, 2, 3 and 4 are used, respectively. The projection of the unknown vector  $u$  on a microphone vector is:

$$V_d = u^T \cdot Q \quad (19)$$

where

$$Q = \left( \frac{P_1 \ P_2 \ P_3 \ P_4}{\|P_1\| \|P_2\| \|P_3\| \|P_4\|} \right)^T \quad (20)$$

It is assumed that a point  $(x, y, z)$  is the instantaneous position of the moving object when the wave is incident on the surface of the object. The microphone vectors  $p_1 = -[x - n, y, z]^T$ ,  $p_2 = -[x + n, y, z]^T$ ,  $p_3 = -[x, y, z - m]^T$ , and  $p_4 = -[x, y, z + m]^T$  have a magnitude of the form  $\|p\| = \sqrt{p^T p}$ . Now, the proposed system has four equations and only three unknown variables. In general,  $v$  can be projected onto the column space of a four-by-three matrix. Therefore,  $u$  can be estimated by the linear-least-squares approach [32].

$$u = (H^T H)^{-1} H^T W v_d \quad (21)$$

where

$$H = \begin{bmatrix} \frac{(x-n)}{\|P_1\|} & \frac{y}{\|P_1\|} & \frac{z}{\|P_1\|} \\ \frac{x+n}{\|P_2\|} & \frac{y}{\|P_2\|} & \frac{z}{\|P_2\|} \\ \frac{x}{\|P_3\|} & \frac{y}{\|P_3\|} & \frac{z-m}{\|P_3\|} \\ \frac{x}{\|P_4\|} & \frac{y}{\|P_4\|} & \frac{z+m}{\|P_4\|} \end{bmatrix} \quad (22)$$

and

$$W = \frac{1}{4} \begin{bmatrix} 1 & 1 & 1 & 1 \\ 1 & 1 & 1 & 1 \\ 1 & 1 & 1 & 1 \\ 1 & 1 & 1 & 1 \end{bmatrix} \quad (23)$$

$H$  is an observation matrix, and  $W$  is a weighted averaging matrix.

## 4. Evaluation and Results for Proposed System

### 4.1. Experimental setup

The experimental setup for the 3D position and velocity measurements is pictured in Fig. 5. In this experiment, the frequency of the transmitted LPM signal sweeps from 50 kHz to 20 kHz. The length of the transmitted LPM signal is 3.274 ms. A pair of LPM signals are generated from a function generator at  $4 V_{p-p}$  and enlarged by an amplifier with a factor of 10. A loudspeaker emits the LPM signal to the spherical object with a 10 cm diameter. The echoed signals are derived by the four acoustical receivers made from silicon MEMS. This model can sense sound pressure or particle velocity in all directions (i.e., it is omnidirectional) [9, 33-34]. The allowed frequencies range from 10 kHz to 100 kHz. As such, the sensor is embedded into a signal processing board with a low-pass frequency circuit with a 60 kHz frequency cutoff and a preamplifier of 20 dB. The minimum sensitivity level of the sensor is -47 dB when the humidity does not exceed 70 R.H. The distance between the Pioneer PT-R4 loudspeaker and the microphones is 10 cm on the X-axis. On the other hand, the distance to the microphones on the Z-axis is 11 cm.



Fig. 9, and the averages and standard deviations are shown in Fig. 13. Averages of the distance, the elevation angle, and the azimuth angle for the fourth position are 93.4 cm, 12.4°, and 121.9°, respectively. The maximum standard deviations of the distance, the elevation angle, and the azimuth angle for the fourth position are 0.033 cm, 0.377°, and 0.547°, respectively.

The object employed in the experiments is a rigid body, but it is assumed that the object is a point for the proposed method. The surface of the object on which the sound is incident is estimated as the measurement point because the exact reference point at the center of the rigid body cannot be known. The exact reference point is unpredictable on the rigid body. For this reason, deviations between the reference point and the measurement point are observed. Therefore, measurement fluctuations are dependent on the direction of the sound beam propagation from the sound source to the target and the object's shape. From the experimental results for the four object positions, it is noticed that the distance ( $d$ ) has the relatively smallest variance when compared with the elevation angle ( $\theta$ ) and the azimuth angle ( $\phi$ ). The reason is that the computations from TOFs for the  $\theta$  and  $\phi$  parameters are more sensitive than those for the  $d$  parameter. For the case when the tested object is outside the main sound beam, the range of measurements can be expanded by altering the position of the speaker. The sound beam is shifted up +10° and down -10° from the Z-axis by manually lifting the loudspeaker position, as illustrated in Fig. 14. The variance of these conditions is not different from the case when the object is inside the main sound beam. In addition, when the velocity of the moving object is increased, a greater variance of position measurements is produced. This is likely due to vibrations in the moving object because the motorized stage for driving the object is controlled by an automatic system for repeated evaluations.

For the velocity measurements, the velocity of the moving object measured by four microphones is estimated using 3D velocity vector measurements. The velocity estimation is composed of X, Y, and Z components, which are represented by  $v_x$ ,  $v_y$ , and  $v_z$ . In the experiment, the moving object can be controlled by a motorized stage, which can move only along the Y-axis. Therefore, a reference velocity is set up only for the  $v_y$  component, and  $v_x$  and  $v_z$  are assumed to be zero. The velocity measurement results for the first position are shown in Fig. 15. The  $v_y$  velocity component for the first case agrees with the reference. The  $v_x$  and  $v_z$  velocity components for the first case are between -0.1 to 0.1 m/s and -0.04 to 0.04 m/s, respectively. The velocity measurement results for the second case are shown in Fig. 16. The  $v_y$  velocity component for the second case is smaller than the reference by about  $\pm 0.05$  m/s for the higher velocity. The  $v_x$  and  $v_z$  velocity components for the second case are between -0.11 to 0.11 m/s and -0.15 to 0.15 m/s, respectively.

The velocity measurement results for the third case are shown in Fig. 17. The  $v_y$  velocity component for the third case is smaller than the reference by about  $\pm 0.02$  m/s for the higher velocity. The  $v_x$  and  $v_z$  velocity components for the third case are between -0.02 to 0.02 m/s and -0.08 to 0.08 m/s, respectively. Finally, the velocity measurement results for the fourth case are shown in Fig. 18. The  $v_y$  velocity component for the fourth case is smaller than the reference by about  $\pm 0.04$  m/s at the higher velocity. The  $v_x$  and  $v_z$  velocity components for the fourth case are between -0.04 to 0.04 m/s and -0.02 to 0.02 m/s, respectively. It is noticed that the proposed 3D velocity vector measurement has a less accurate  $v_y$  component when the moving object is elevated higher from the X-Y plane, and the  $v_x$  and  $v_z$  components are not complete zero due to the Doppler velocity estimation from the Doppler-shift length measurements of the received LPM signals at acoustical receivers, as the receivers could not sense the same length of the obtained LPM signal at the same velocity.

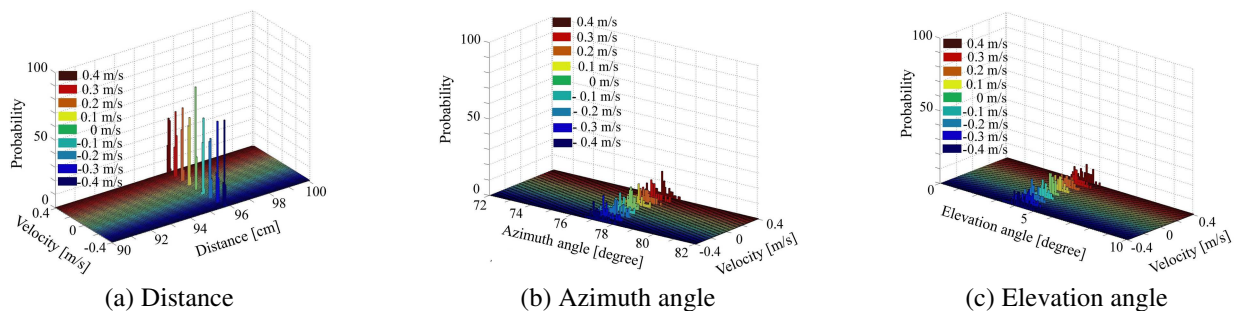


Fig. 6 Experimental results of the determined position at  $d = 96$  cm,  $\phi = 78^\circ$ , and  $\theta = 5^\circ$  when varying the velocity

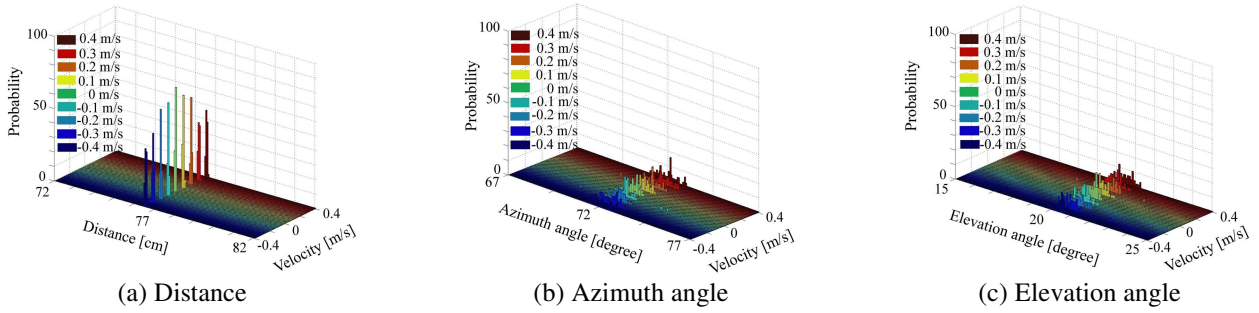


Fig. 7 Experimental results of the determined position at  $d = 78$  cm,  $\phi = 70^\circ$ , and  $\theta = 18^\circ$  when varying the velocity

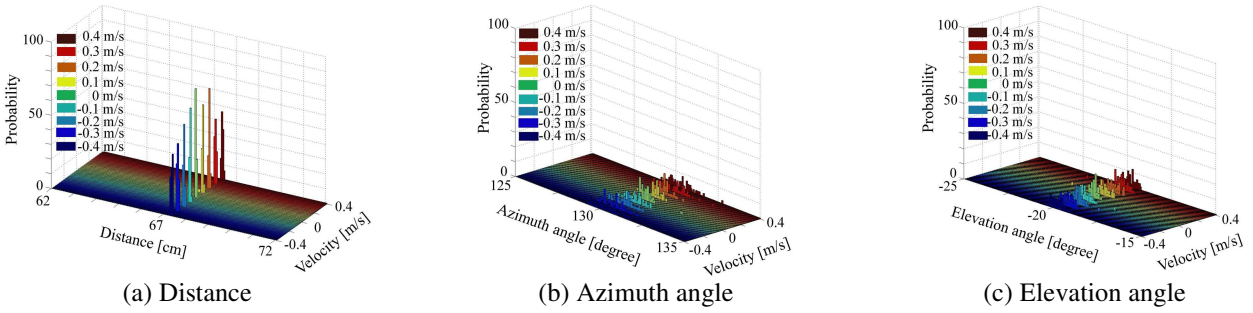


Fig. 8 Experimental results of the determined position at  $d = 65$  cm,  $\phi = 130^\circ$ , and  $\theta = 22^\circ$  when varying the velocity

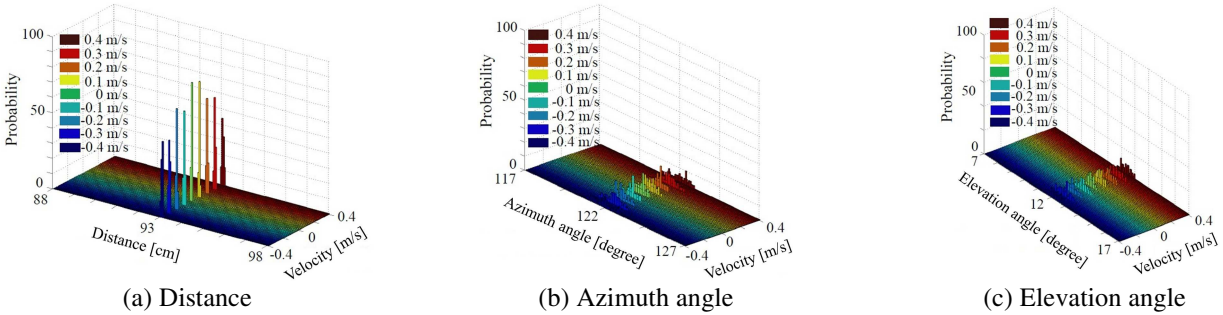


Fig. 9 Experimental results of the determined position at  $d = 91$  cm,  $\phi = 124^\circ$ , and  $\theta = 10^\circ$  when varying the velocity

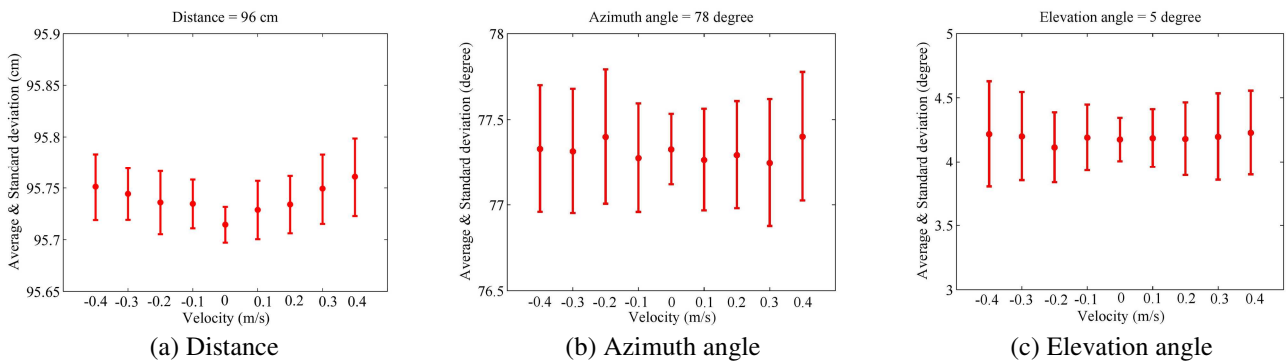


Fig. 10 Averages and standard deviations of the determined position at  $d = 96$  cm,  $\phi = 78^\circ$ , and  $\theta = 5^\circ$  at various velocities

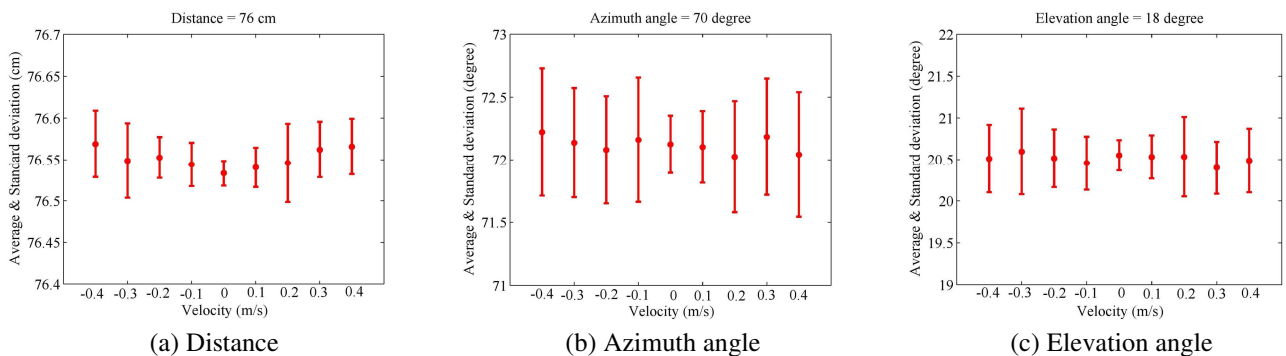


Fig. 11 Averages and standard deviations of the determined position at  $d = 78$  cm,  $\phi = 70^\circ$ , and  $\theta = 18^\circ$  at various velocities

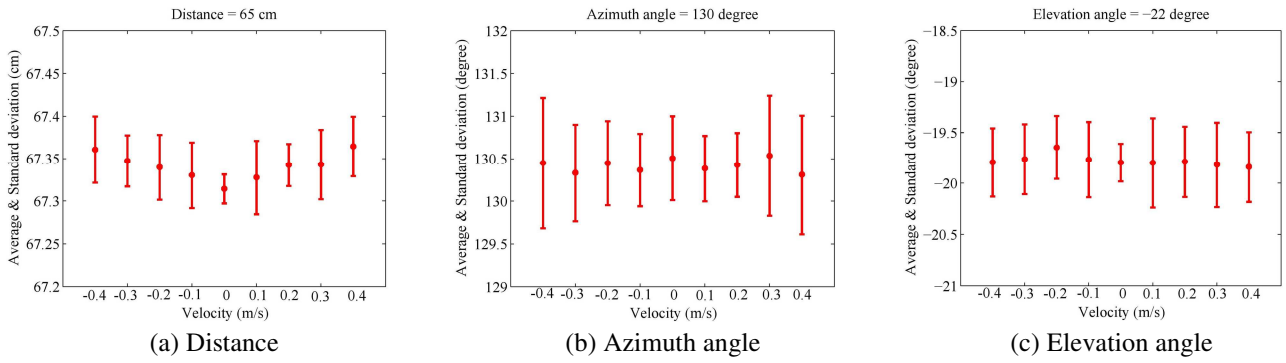


Fig. 12 Averages and standard deviations of the determined position at  $d = 65$  cm,  $\phi = 130^\circ$ , and  $\theta = -22^\circ$  at various velocities

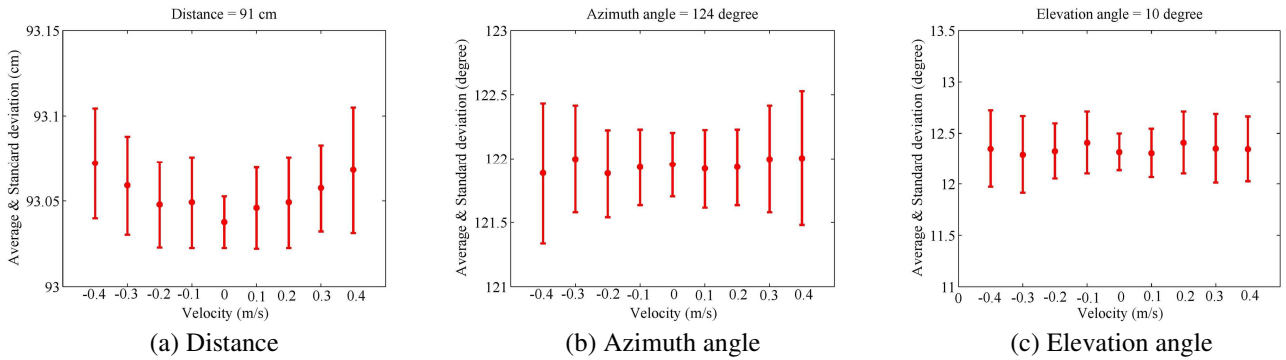


Fig. 13 Averages and standard deviations of the determined position at  $d = 91$  cm,  $\phi = 124^\circ$ , and  $\theta = 10^\circ$  at various velocities

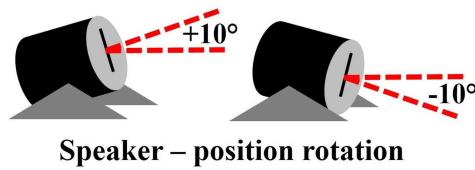


Fig. 14 Sound beam scanning by rotating the speaker

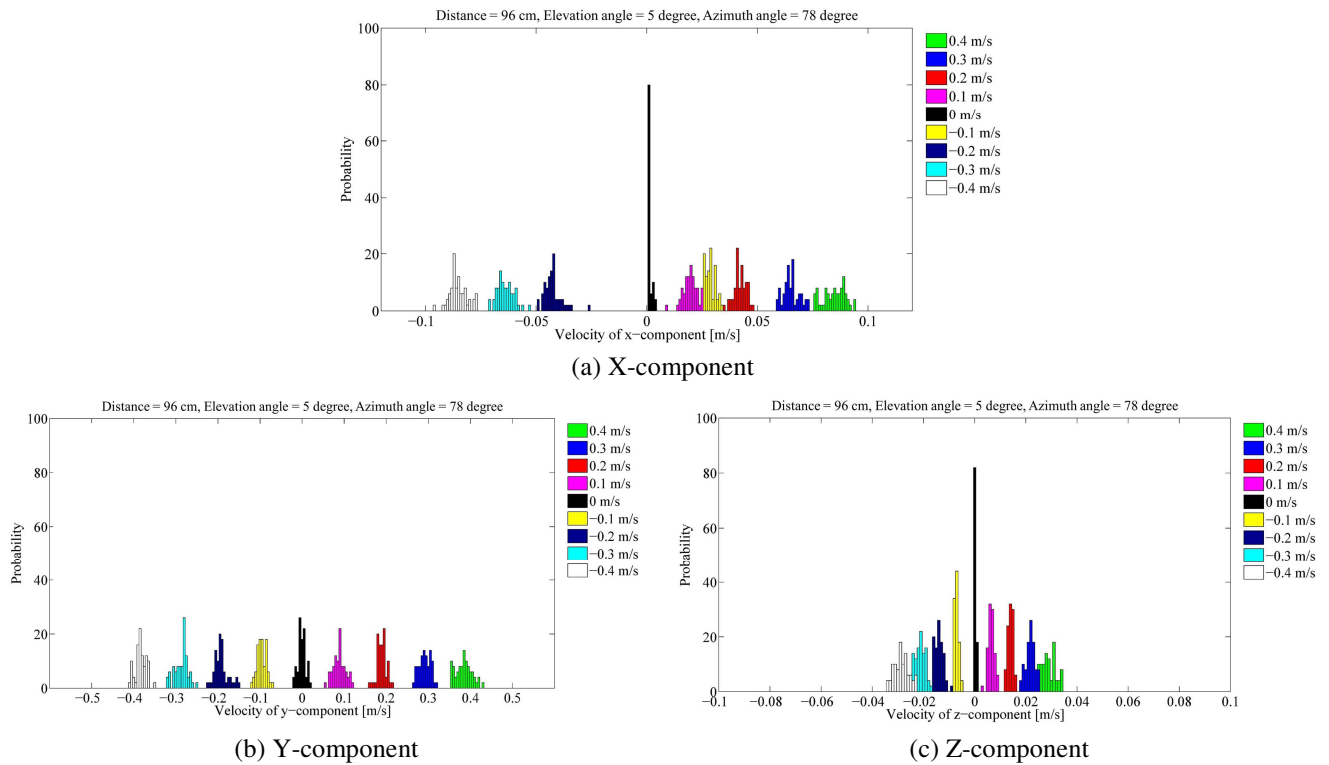


Fig. 15 Vector velocity measurements at  $d = 91$  cm,  $\phi = 124^\circ$ , and  $\theta = 10^\circ$

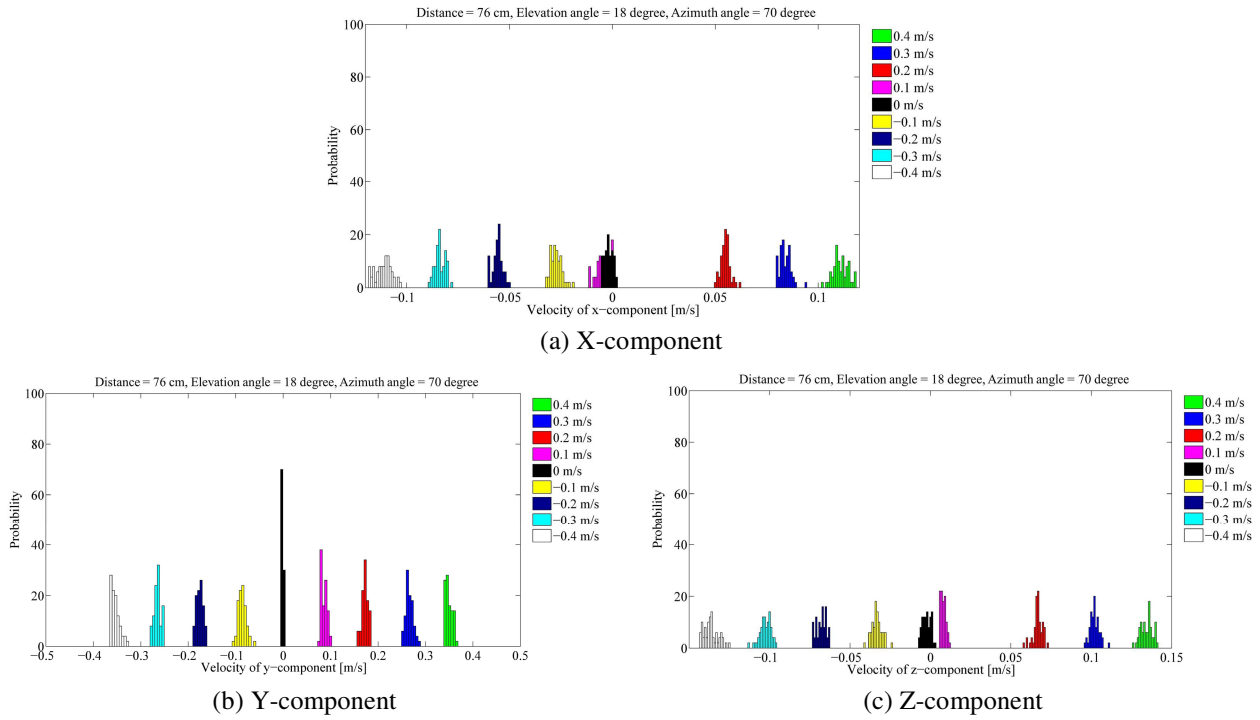


Fig. 16 Vector velocity measurements at  $d = 76$  cm,  $\phi = 18^\circ$ , and  $\theta = 70^\circ$

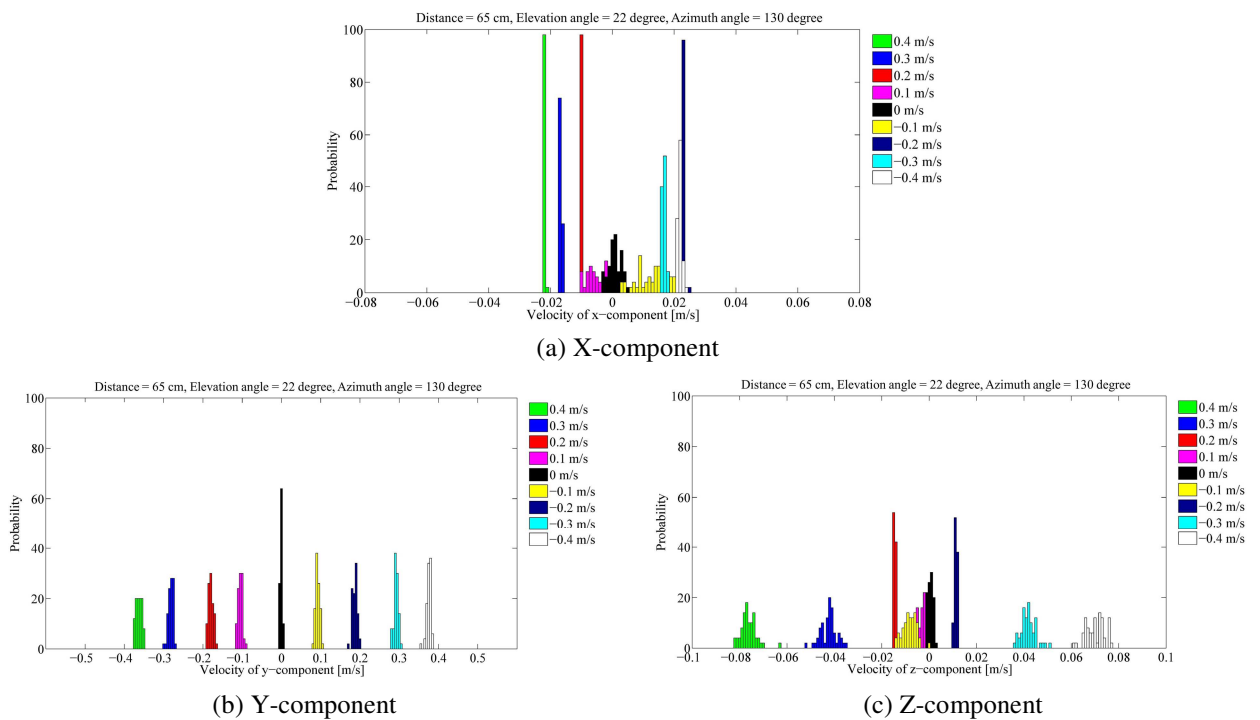


Fig. 17 Vector velocity measurements at  $d = 65$  cm,  $\phi = -22^\circ$ , and  $\theta = 130^\circ$

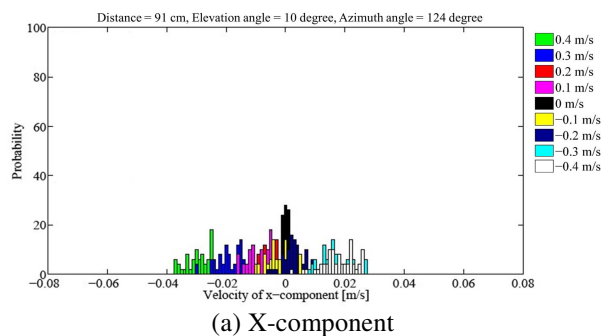


Fig. 18 Vector velocity measurements at  $d = 91$  cm,  $\phi = 10^\circ$ , and  $\theta = 124^\circ$

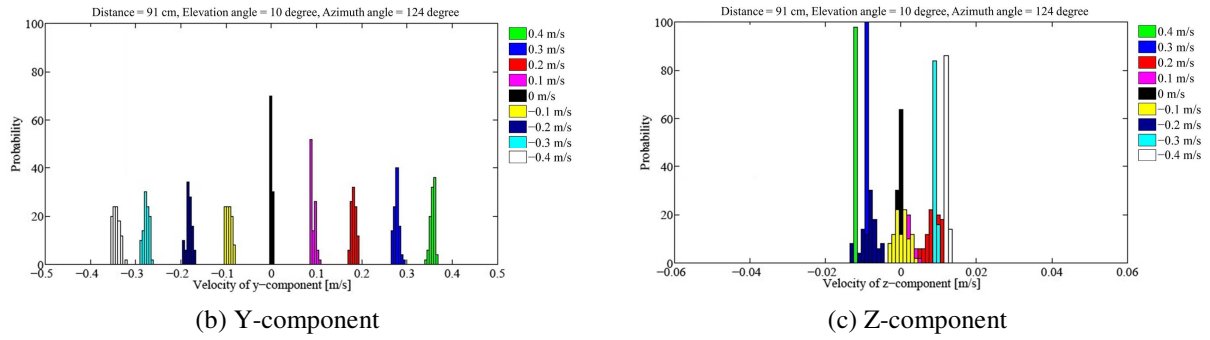


Fig. 18 Vector velocity measurements at  $d = 91$  cm,  $\phi = 10^\circ$ , and  $\theta = 124^\circ$  (continued)

### 5. Conclusions

This study demonstrated the measurement of 3D position and velocity utilizing an oversampling-based signal processing method with an LPM ultrasonic signal. The proposed system consists of a cross-correlation using a one-bit signal processing technique with a low computational time cost. The velocity measurements were computed based on the 3D velocity vector measurements. The object’s position was calculated using spherical coordinates. Positions determined in the proposed system were evaluated by experimental demonstration. The object position can be sensed by the sound beam propagated by a loudspeaker. The probability distributions for 50 trials assessed the accuracy of the developed method for position measurements. The mean value and standard deviations were used to determine the reliability of the measurements. The resolution of the proposed system was approximately  $14 \mu\text{m}$  for a sound velocity of  $345 \text{ m/s}$  and a sampling rate of  $12.5 \text{ MHz}$ . The deviation of the actual results is for a point, but the target was a spherical ball. The reference of the object position was fixed to the center on the surface of the ball.

The velocity estimation was made up of components in the X, Y, and Z directions. In this experiment, the moving object can be forced in only Y-direction movement due to the limitation of the experimental apparatus. However, the technique is still able to estimate the position and velocity of the moving object in 3D space. The validity and repeatability of the experimental results are evaluated by statistical methods, showing  $\pm 1\%$  of accuracy.

### Abbreviations and Symbols

DOA	Direction-of-arrival	$p_b$	Period of the LPM signal
DSD	Direct stream digital	$P_{\max}$	Maximum peak
FIR	Finite impulse response	$P_{\min}$	Minimum peak
FPGA	Field-programmable gate arrow	$p_s$	Starting time of the sweeping period
LFM	Linear-frequency-modulated	$s$	Reference LPM one-bit signal
LPM	Linear-period-modulated	$t_e$	Compensated peak time
SACD	Super audio CD	$t_{\max}$	Time at maximum peak
SNR	Signal-to-noise ratio	$t_{\min}$	Time at minimum peak
TOF	Time-of-flight	$u$	Velocity vector of the moving object
3D	Three-dimensional	$v$	Propagation velocity of a sound wave in the air
$c$	Cross-correlation function	$v_d$	Doppler velocity
$d$	Distance from the loudspeaker to the object	$V_d$	Relative-Doppler velocity measurements
$f$	Original LPM signal	$x$	Echo signal in one-bit stream
$H$	Observation matrix	$W$	Weighted averaging
$l$	Natural number	$Z$	Zero cross point
$l_d$	Doppler-shift length of the received LPM signal	$2n$	Distance between microphones 3 and 4
$l_0$	Reference LPM signal length	$\zeta$	Doppler velocity coefficient
$M$	Huge number	$\theta$	Elevation angle
$p$	Microphone vector	$\phi$	Angle of azimuth

## Acknowledgements

This research was funded by Faculty of Engineering, King Mongkut's University of Technology North Bangkok Contract no. ENG-64-106.

## Conflicts of Interest

The authors declare no conflict of interest.

## References

- [1] S. P. Dear, J. A. Simmons, and J. Fritz, "A Possible Neuronal Basis for Representation of Acoustic Scenes in Auditory Cortex of the Big Brown Bat," *Nature*, vol. 346, pp. 620-623, August 1993.
- [2] W. Wongsaroj, H. Takahashi, N. Thong-Un, and H. Kikura, "Ultrasonic Measurement for the Experimental Investigation of Velocity Distribution in Vapor-Liquid Boiling Bubbly Flow," *International Journal of Engineering and Technology Innovation*, vol. 12, no. 1, pp. 16-28, January 2022.
- [3] P. Pal, "Dynamic Poisson's Ratio and Modulus of Elasticity of Pozzolana Portland Cement Concrete," *International Journal of Engineering and Technology Innovation*, vol. 9, no. 2, pp. 131-144, March 2019.
- [4] F. E. Gueuning, M. Varlan, C. E. Eugene, and P. Dupuis, "Accurate Distance Measurement by an Autonomous Ultrasonic System Combining Time-of-Flight and Phase-Shift Methods," *IEEE Instrumentation and Measurement Technology Conference*, pp. 1236-1240, June 1996.
- [5] R. Queiros, F. C. Alegria, P. S. Girao, and A. C. Serra, "Cross-Correlation and Sine-Fitting Techniques for High-Resolution Ultrasonic Ranging," *IEEE Transactions on Instrumentation and Measurement*, vol. 59, no. 12, pp. 3227-3236, April 2006.
- [6] X. F. Wang and Z. A. Tang, "A Novel Method for Digital Ultrasonic Time-of-Flight Measurement," *Review of Scientific Instruments*, vol. 81, 105112, October 2010.
- [7] D. Marioli, C. Narduzzi, C. Offelli, D. Petri, E. Sardini, and A. Taroni, "Digital Time-of-Flight Measurement for Ultrasonic Sensors," *IEEE Transactions on Instrumentation and Measurement*, vol. 41, no. 1, pp. 93-97, February 1992.
- [8] J. M. Martin, A. R. Jiménez, F. Seco, L. Calderón, J. L. Pons, and R. Ceres, "Estimating the 3D-Position from Time Delay Data of US-Waves Experimental Analysis and a New Processing Algorithm," *Sensors and Actuators A: Physical*, vol. 101, no. 3, pp. 311-321, October 2002.
- [9] N. Thong-Un, S. Hirata, and M. Kurosawa, "Three-Dimensional-Positioning Based on Echolocation Using a Simple Iterative Method," *AEÜ—International Journal of Electronics and Communications*, vol. 69, no. 3, pp. 680-684, March 2015.
- [10] S. Noykov and C. Roumenin, "Calibration and Interface of a Polaroid Ultrasonic Sensor for Mobile Robots," *Sensors and Actuators A: Physical*, vol. 135, no. 1, pp. 169-178, March 2007.
- [11] J. M. Abreu, R. Ceres, L. Calderon, M. A. Jiménez, and P. Gonzales-de-Santos, "Measuring the 3D-Position of a Walking Vehicle Using Ultrasonic and Electromagnetic Waves," *Sensors and Actuators A: Physical*, vol. 75, no. 2, pp. 131-138, May 1999.
- [12] N. Thong-Un, S. Hirata, M. K. Kurosawa, and Y. Orino, "Three-Dimensional Position and Velocity Measurements Using a Pair of Linear-Period-Modulated Ultrasonic Waves," *Acoustical Science and Technology*, vol. 34, no. 3, pp. 233-236, May 2013.
- [13] K. Mannay, J. Ureña, A. Hernández, J. M. Villadangos, M. Machhout, and T. Aguilí, "Evaluation of Multi-Sensor Fusion Methods for Ultrasonic Indoor Positioning," *Applied Sciences*, vol. 11, no. 15, 6805, July 2021.
- [14] B. Kreczmer, "Objects Localization and Differentiation Using Ultrasonic Sensor", <https://www.intechopen.com/chapters/10581>, March 01, 2010.
- [15] D. Klimentjew, N. Hendrich, and J. Zang, "Multi Sensor Fusion of Camera and 3D Laser Range Finder for Object Recognition," *IEEE Conference on Multisensor Fusion and Integration*, pp. 236-241, October 2010.
- [16] M. Pollakowski and H. Ermert, "Chirp Signal Matching and Signal Power Optimization in Pulse-Echo Mode Ultrasonic Nondestructive Testing," *IEEE Transactions on Ultrasonics, Ferroelectrics, and Frequency Control*, vol. 41, no. 5, pp. 655-659, September 1994.

- [17] H. Matsuo, T. Yamaguchi, and H. Hachiya, "Target Detectability Using Coded Acoustic Signal in Indoor Environments," *Japanese Journal of Applied Physics*, vol. 47, no. 5, 4325, May 2008.
- [18] R. A. Altes, "Sonar Velocity Resolution with a Linear-Period-Modulated Pulse," *The Journal of the Acoustical Society of America*, vol. 61, no. 4, pp. 1019-1030, 1977.
- [19] J. J. Kroszczynski, "Pulse Compression by Means of Linear-Period Modulation," *Proc. of the IEEE*, vol. 57, no. 7, pp. 1260-1266, July 1969.
- [20] S. Hirata and M. K. Kurosawa, "Ultrasonic Distance and Velocity Measurement Using a Pair of LPM Signals for Cross-Correlation Method: Improvement of Doppler-Shift Compensation and Examination of Doppler Velocity Estimation," *Ultrasonics*, vol. 52, no. 7, pp. 873-879, September 2012.
- [21] S. Hirata, T. Sato, M. K. Kurosawa, and T. Katagiri, "Ultrasonic Distance and Velocity Measurement Using a Pair of Linear-Period-Modulated Signals Coding by Maximum Length Sequences for Autonomous Mobile Robots," 16th International Congress on Sound and Vibration, pp. 1-8, July 2009.
- [22] Royal Philips Electronics and Sony Corporation, "Super Audio CD Production Using Direct Stream Digital Technology," [https://www.merging.com/uploads/assets/Merging\\_pdfs/dsd1.pdf](https://www.merging.com/uploads/assets/Merging_pdfs/dsd1.pdf), 2000.
- [23] S. Hirata, M. K. Kurosawa, and T. Katagiri, "Accuracy and Resolution of Ultrasonic Distance Measurement with High-Time-Resolution Cross-Correlation Function Obtained by Single-Bit Signal Processing," *Acoustical Science and Technology*, vol. 30, no. 6, pp. 429-438, November 2009.
- [24] S. Saito, M. K. Kurosawa, Y. Orino, and S. Hirata, "Airborne Ultrasonic Position and Velocity Measurement Using Two Cycles of Linear-Period-Modulated Signal," *Proc. of 12th Towards Autonomous Robotic Systems*, pp. 46-53, July 2011.
- [25] N. Thong-Un, S. Hirata, and M. K. Kurosawa, "Improvement in Airborne Position Measurements Based on an Ultrasonic Linear-Period-Modulated Wave by 1-Bit Signal Processing," *Japanese Journal of Applied Physics*, vol. 54, no. 7S1, 07HC06, June 2015.
- [26] M. Navarro and M. Najar, "TOA and DOA Estimation for Positioning and Tracking in IR-UWB," *IEEE International Conference on Ultra-Wideband*, pp. 574-579, September 2007.
- [27] A. Lazarov, D. Minchev, and A. Dimitrov, "Ultrasonic Positioning System Implementation and Dynamic 3D Visualization," *Cybernetics and Information Technologies*, vol. 17, no. 2, pp. 151-163, June 2017.
- [28] Z. Chen, G. Gokeda, and Y. Yu, *Introduction to Direction-of-Arrival Estimation*, Boston: Artech House, 1990.
- [29] S. Hirata, M. K. Kurosawa, and T. Katagiri, "Cross-Correlation by Single-Bit Signal Processing for Ultrasonic Distance Measurement," *IEICE Transactions on Fundamentals of Electronics, Communications, and Computer Sciences*, vol. E91-A, no. 4, pp. 1031-1037, April 2008.
- [30] L. Beranek, *Acoustics*, New York: Acoustic Society of America, 1996.
- [31] H. Krim and M. Viberg, "Two Decades of Array Signal Processing Research: The Parametric Research," *IEEE Signal Processing Magazine*, vol. 13, no. 4, pp. 67-94, July 1996.
- [32] S. M. Kay, *Fundamentals of Statistical Signal Processing Acoustics*, New Jersey: Prentice Hall, 1993.
- [33] N. Thong-Un, S. Hirata, M. K. Kurosawa, and Y. Orino, "Three-Dimensional-Positioning Measurements Based on Echolocation using Linear-Period-Modulated Ultrasonic Signal," *IEEE International Ultrasonics Symp.*, pp. 2478-2481, September 2014.
- [34] K. Mizutani, T. Ito, M. Sugimoto, and H. Hashizume, "TSaT-MUSIC: A Novel Algorithm for Rapid and Accurate Ultrasonic 3D Localization," *EURASIP Journal on Advances in Signal Processing*, vol. 2011, 101, November 2011.



Copyright© by the authors. Licensee TAETI, Taiwan. This article is an open access article distributed under the terms and conditions of the Creative Commons Attribution (CC BY-NC) license (<https://creativecommons.org/licenses/by-nc/4.0/>).